

Thermal-neutron cross sections and resonance integrals of ^{138}Ba and ^{141}Pr using Am-Be neutron source

Priyada Panikkath^a and P. Mohanakrishnan

Manipal Centre for Natural Sciences, Manipal University, Karnataka-576104, India

Received: 25 May 2016 / Revised: 22 July 2016

Published online: 12 September 2016 – © Società Italiana di Fisica / Springer-Verlag 2016

Communicated by R.K. Bhandari

Abstract. The thermal-neutron capture cross sections and resonance integrals of $^{138}\text{Ba}(n, \gamma)^{139}\text{Ba}$ and $^{141}\text{Pr}(n, \gamma)^{142}\text{Pr}$ were measured by activation method using an isotopic Am-Be neutron source. The estimations were with respect to that of $^{55}\text{Mn}(n, \gamma)^{56}\text{Mn}$ and $^{197}\text{Au}(n, \gamma)^{198}\text{Au}$ reference monitors. The measured thermal-capture cross section of ^{138}Ba with respect to ^{55}Mn is 0.410 ± 0.023 b and with respect to ^{197}Au is 0.386 ± 0.019 b. The measured thermal-capture cross section of ^{141}Pr with respect to ^{55}Mn is 11.36 ± 1.29 b and with respect to ^{197}Au is 10.43 ± 1.14 b. The resonance integrals for ^{138}Ba are 0.380 ± 0.033 b (^{55}Mn) and 0.364 ± 0.027 b (^{197}Au) and for ^{141}Pr are 21.05 ± 2.88 b (^{55}Mn) and 15.27 ± 1.87 b (^{197}Au). The comparison between the present measurements and various reported values are discussed. The cross sections corresponding to the selected isotopes are measured using an Am-Be source facility for the first time.

1 Introduction

Nuclear data, especially the neutron capture cross sections and resonance integrals of various target nuclides are required in diverse areas including fundamental nuclear science, astrophysics, condensed matter physics and reactor physics. The present knowledge of nuclear data especially of neutron-induced reactions need to be updated with new experimental, theoretical or simulation based studies to reduce the uncertainties in the design and operation of new generation reactors. The sparseness in and spread among different cross section measurements are still found to be large [1] compared to the requirement (uncertainty $\leq 5\%$) for different applications. The need for comprehensive studies for obtaining nuclear data with reduced uncertainties is emphasized in recent articles [2,3]. Neutron activation is one of the widely employed methods for measurement of neutron cross sections and resonance integrals. Generally, reactor neutron beam or D-T neutron beam is used for such activation measurements. However, in last few decades the use of isotopic neutron sources such as Am-Be for cross section measurements has been established [4,5].

The present study focuses on the measurement of thermal-neutron capture cross sections and resonance integrals of $^{138}\text{Ba}(n, \gamma)^{139}\text{Ba}$ and $^{141}\text{Pr}(n, \gamma)^{142}\text{Pr}$ using the Am-Be neutron source. ^{138}Ba and ^{141}Pr are selected for the present study because of their importance as the fission products in the thermal-neutron-induced fission of

^{235}U and fast-neutron-induced fission of ^{239}Pu . Therefore, the accurate nuclear data especially of neutron capture reactions of these isotopes are required in nuclear fuel cycle, reactor safety and burn-up calculations. After a careful and thorough literature survey using EXFOR [6] database, the following observations are made regarding the thermal-neutron capture cross sections and resonance integrals of ^{138}Ba and ^{141}Pr . Barium (^{138}Ba) is one of such isotopes where the resonance integral measured recently are discrepant from the evaluated data. The measured resonance integral values of $^{138}\text{Ba}(n, \gamma)^{139}\text{Ba}$ spread in the range 0.256 b–0.382 b, whereas the evaluations by Mughabghab, ENDF-B.VII and EAF-2010 are 0.32 b, 0.265 b and 0.263 b, respectively [7–9]. Most of the measured thermal-neutron capture cross sections of ^{138}Ba reported (0.23 b–0.68 b) are also different from the evaluated value (0.404 b) [7]. There are discrepancies between different evaluations also. Praseodymium (^{141}Pr) is one such isotope where most of the measured data are old except the one by Yoon *et al.* [10]. As per the database, there are eight measured thermal-neutron capture cross section data for ^{141}Pr which vary between 8.36 b to 11.6 b where as the evaluated data is near the upper limit of 11.5 b [7]. The evaluated resonance integral values of $^{141}\text{Pr}(n, \gamma)^{142}\text{Pr}$ are in the range 17.4–17.9 b having a good agreement with each other [7–9]. However, the measured resonance integrals are spread over a wide range (9.3 b–21.4 b) and there is a lack of recent measurement. The agreement between the different evaluations is better in ^{141}Pr compared to ^{138}Ba . These observations indicate the necessity of more

^a e-mail: priyadapv@gmail.com

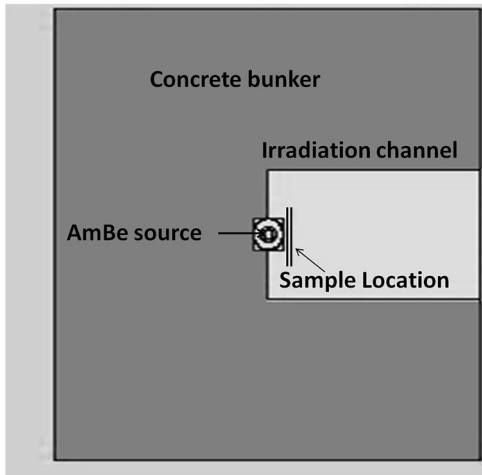


Fig. 1. Schematic of the cross sectional view of irradiation facility.

accurate measurements of thermal-neutron capture cross section and resonance integral of the above-mentioned isotopes.

The thermal-neutron capture cross sections and resonance integrals are estimated relative to that of $^{55}\text{Mn}(n, \gamma)^{56}\text{Mn}$ and $^{197}\text{Au}(n, \gamma)^{198}\text{Au}$ reference monitors. There are no measured data available for $^{138}\text{Ba}(n, \gamma)^{139}\text{Ba}$ and $^{141}\text{Pr}(n, \gamma)^{142}\text{Pr}$ using Am-Be facility as per the authors knowledge. The advantages of isotopic source facility relative to reactor are convenience and comparative easy availability. The disadvantage of lower irradiation flux level is offset partly by longer irradiations and larger samples. The experimental setup, procedure and data analysis followed are explained in the subsequent sections. In order to determine the spectrum independent resonance integral, epithermal shape factor is also estimated from the experimental neutron spectrum. A Monte Carlo based simulation method is followed in estimating the thermal and epithermal self-shielding correction factors of all the targets.

2 Experimental methods

All the samples were irradiated at the neutron physics lab at Manipal Centre for Natural Sciences, Manipal University. The Am-Be source emits 4×10^7 neutrons per second in 4π direction. The neutron spectrum gets moderated due to the concrete shield around the neutron source. The samples were placed close to the neutron source and the neutron spectrum at this location has mixed components including thermal, epithermal and fast. Thermal component of neutron spectrum ($E \leq 0.55$ eV) is maximum at this location and is around 5×10^3 n/cm²/s and the epithermal component (0.55 eV $< E \leq 100$ keV) is approximately 7×10^3 n/cm²/s. A schematic of the cross sectional view of the irradiation facility is shown in fig. 1. Activation foils of Mn (Mn(83%)-Cu) and Au having 12 mm diameter procured from Shieldwerx with purity 99.9% were used as reference isotopes. Analytical grade powder samples of BaCl₂ (Merck make) and Pr₆O₁₁ (procured from

Star rare earth limited) were used for the cross section measurements. The powder samples were made into circular packets of diameter 12 mm. Weight of each samples prepared were indicated in table 1. In order to achieve measurable activity, the amount of BaCl₂ used for irradiation is higher compared to the other samples owing to the lower cross section of $^{138}\text{Ba}(n, \gamma)^{139}\text{Ba}$. Two sets of each sample were used in the experiment; one of each was irradiated by enclosing in a cadmium cover and other without cadmium cover. Standard cadmium covers provided by Shieldwerx is used in the experiment. All the foils were irradiated placing together side by side for 7 days. The distance between the foils was around 10 mm in order to avoid the flux depression due to the presence of Cd. The irradiations were repeated with another set of samples with similar dimensions for a longer duration of 15 days.

After irradiation the induced activity in each of the samples were counted using a well shielded 30% efficiency HPGe (Bruker Baltic) detector having an energy resolution of 0.25% at 1.33 MeV. The distance between the foil and the detector was 2 cm considering the low counting rate. There is only one gamma peak with higher yield in the decay scheme of the foils of the present study. Moreover, the activity produced will be very much smaller for any coincidence summing effect to be present. Hence, the effect of coincidence summing is neglected in the present measurements. The energy and efficiency of the detector was pre-calibrated using the gamma lines from ^{152}Eu . Gamma lines of interest (E_γ) from the capture products of the various samples and reference monitors along with other important data used in the present analysis are listed in table 1. Counting duration for each of the samples was varied in the range 7200 s–80000 s based on the counting rate as well as the half life of the decaying isotope such that a satisfactory counting statistics is achieved. The net areas (C) under the full peaks of energies mentioned in table 1 are obtained from the background subtracted gamma spectra. Reaction rate per target atom (R) is estimated from these net areas using the following relation:

$$R = \frac{C\lambda_c}{[1 - e^{-\lambda t_{irr}}][e^{-\lambda t_d}][1 - e^{-\lambda t_c}]} \frac{Mf}{N_A \theta \epsilon I_\gamma m}, \quad (1)$$

where λ is the decay constant in s⁻¹, t_{irr} is the irradiation duration, t_d is the delay time, t_c is the counting time, ϵ is efficiency of the detector, I_γ is gamma yield, N_A is Avogadro number, θ is the isotopic abundance, f is the correction factor for gamma attenuation, m is the weight of the target and M is the atomic mass of the target. The correction factor, f is determined using the relation $f = \mu x / (1 - e^{-\mu x})$, where x is the thickness of the sample and μ is the linear attenuation coefficient which is energy and material dependent. Linear attenuation coefficients corresponding to the appropriate energies are obtained with the help of XCOM photon data base [11].

2.1 Estimation of self-shielding correction factors

When a sample is being irradiated in neutron field, its presence can cause perturbation to the neutron flux. A

Table 1. Nuclear data and parameters of the samples used in the calculations [12–15].

Reaction	Foil/Sample	Weight (mg)	E_γ (keV)	I_γ (%)	$T_{1/2}$	Er (eV)	F_{Cd}	f	g	σ_0 (b)	I (b)
$^{197}\text{Au}(n, \gamma)^{198}\text{Au}$	Au	125 ± 0.6	411.5	95.6 ± 0.12	2.69 d	5.47	1.009	1.009	1.0054	98.71	1563
$^{55}\text{Mn}(n, \gamma)^{56}\text{Mn}$	Mn(83%)-Cu	40 ± 0.2	846.7	98.85 ± 0.3	2.58 h	468	1	1.005	1.0003	13.41	11.76
$^{138}\text{Ba}(n, \gamma)^{139}\text{Ba}$	BaCl ₂	1000 ± 2	165.8	23.7 ± 0.24	83.06 m	15700	1	1.21	0.9993	–	–
$^{141}\text{Pr}(n, \gamma)^{142}\text{Pr}$	Pr ₆ O ₁₁	55 ± 0.1	1576	3.7 ± 0.4	19.12 h	296	1	1.03	1.0003	–	–

depression in neutron flux will appear corresponding to resonance peaks and an enhancement in the flux will appear due to sudden minima in cross sections. This change in reaction rate due to sample presence is known as self-shielding of the foil. It can be estimated from the ratio of reaction rate produced in the sample to reaction rate produced in an infinitely diluted sample.

There are analytical methods to estimate the thermal self-shielding correction factor and epithermal self-shielding correction factor [16–19]. The macroscopic cross section and the thickness of the foil are used to estimate the thermal self-shielding correction factor analytically [17]. In order to estimate the resonance self-shielding correction factor, macroscopic total cross section and the ratio between capture width to total width at the most prominent resonance energy are utilized [18]. These analytical methods are universal irrespective to the irradiation channel. However, the self-shielding correction factors specific to the irradiation channel can be estimated using the Monte Carlo method by incorporating the experimental setup accurately. Hence, in the present work the self-shielding correction factors are estimated from the reaction rates simulated using the Monte Carlo code MCNP [20, 21] and compared with the values calculated analytically as described in ref. [19].

Neutron spectrum at the irradiation location was simulated using the MCNP taking care of the geometrical details. The resultant spectrum is used as the incident plane isotropic source distribution along with the exact dimension and material properties of the foils under irradiation to estimate the reaction rates in the sample. Neutron flux in the sample is estimated using track length estimator tally (F4) and modified using a perturbation tally (FM4) using the capture cross sections from JEFF 3.1 [22]. Reaction rates are estimated for an infinite dilution sample by changing the material density to 0.001 g/cm^3 . While estimating the reaction rates, no structural material is incorporated in the simulation in order to avoid the scattering effects. However, the scattering effects were taken care while simulating the neutron spectrum at the irradiation location. Reaction rates are further classified into the energy range 10^{-9} MeV – $5.5 \times 10^{-7} \text{ MeV}$ and $5.5 \times 10^{-7} \text{ MeV}$ – 12 MeV to estimate thermal self-shielding correction factor (G_{th}) and epithermal self-shielding correction factor (G_{epi}), respectively. The self-shielding factors estimated using the MCNP simulation are compared with those estimated using analytical formula in table 2. A good agreement between both methods is seen especially for thermal

Table 2. Thermal self-shielding correction factors (G_{th}) and epithermal self-shielding correction factors (G_{epi}) of the samples under study estimated using Monte Carlo method and analytical formula.

Foil	Monte Carlo method		Analytical method	
	G_{th}	G_{epi}	G_{th}	G_{epi}
^{197}Au	0.97 ± 0.01	0.27 ± 0.01	0.98	0.27
^{55}Mn	0.99 ± 0.01	1.06 ± 0.01	0.99	0.93
^{138}Ba	1.00 ± 0.01	1.01 ± 0.01	0.99	0.95
^{142}Pr	0.97 ± 0.01	0.60 ± 0.02	0.98	0.66

self-shielding correction factors. The self-shielding correction factors estimated using the MCNP method are used in the subsequent calculations.

2.2 Estimation of epithermal spectrum shape factor

In an ideal moderated (*i.e.*, no absorption of neutrons) neutron spectrum, epithermal flux is proportional to the neutron energy as $\frac{1}{E}$. However, a real neutron spectrum deviates from this dependency and the estimate of this deviation is known as the epithermal spectrum shape factor represented by α . In a real spectrum, the epithermal neutron flux may be represented by a function of energy as $\frac{1}{E^{1+\alpha}}$. Cadmium covered multi monitor method, cadmium ratio of dual monitor method and the cadmium ratio of multi-monitor method are the widely used techniques for accurate determination of α [23–25]. The accuracy will be superior in the case of multi monitor method compared to the dual monitor method. Computer codes for reactor spectrum unfolding based on multifoil activation technique is another possible way of obtaining the epithermal spectrum and thus the shape factor [26]. In the present study spectrum unfolding from multifoil activation is utilised to determine the α . Various foils of (n, γ)[Au, In, Mn, Sc, Cu, Mo, Na], (n, p)[Fe, Ni] and (n, α)[Al] reactions are irradiated in the experimental facility. Reaction rates of all these foils were corrected for self-shielding effect and used to unfold the neutron spectra using SAND II code [27, 28]. In this code the required spectrum is obtained by adjusting with the guess spectrum using the iterative method. The results of the SAND-II code depends crucially on the *a priori* guess spectrum

supplied. In the present case neutron spectrum obtained using the MCNP simulation as shown in fig. 2 is used as the guess spectrum. Neutron energies from 10^{-10} MeV to 18 MeV are divided into 620 groups and the corresponding cross section data are also provided as input. Reaction rates are calculated with the guess spectrum and the cross sections. Measured reaction rates are compared with the calculated reaction rates and the guess spectrum is adjusted to improve the agreement between prediction and measurement. This procedure continues till convergence or user defined accuracy is achieved. In the present case the iteration continued till convergence and the standard deviation between the measured reaction rates and the calculated reaction rates is 3.68%. Once the neutron spectrum is unfolded, epithermal spectrum shape factor α is determined by fitting the spectrum using a non linear relation of the form $\phi(E) = A \times \frac{1}{E^{1+\alpha}}$ in the energy range 0.55 eV–100 keV.

Figure 2 shows the neutron spectra unfolded using SAND II code as well as the non-linear fit line. Spectrum shape factor α is estimated as -0.148 ± 0.007 and it is used in further calculations for estimating the resonance integral. The sharp reduction in the flux near 2 keV is probably due to the iron capture resonance absorption in the surrounding concrete. A direct comparison between the SAND II unfolded spectrum and the simulated guess spectrum is not possible due the difference in energy binning. However, the total neutron flux obtained from SAND II method is 5.39×10^4 n/cm²/s and from the MCNP simulation is 5.7×10^4 n/cm²/s. Similarly, the thermal to total neutron ratio obtained from SAND II method and Monte Carlo simulations are 0.134 and 0.138 respectively. These observations show the agreement between SAND II unfolded spectra and the MCNP simulated spectra. This indicates that the experimental geometry as well as the materials are incorporated faithfully in the Monte Carlo simulation.

3 Formulation of thermal capture and resonance integral

The thermal-neutron capture cross sections and the resonance integrals are determined from the reaction rates measured from the induced activities of the irradiated foils using gamma spectroscopy. The thermal-neutron capture cross section of the sample is determined relative to that of reference sample using eq. (2) [4, 5]

$$\sigma_{0,S} = \frac{(R - \frac{R_{Cd}}{F_{Cd}})_S (G_{th})_S}{(R - \frac{R_{Cd}}{F_{Cd}})_{Rf} (G_{th})_{Rf}} \frac{g_S}{g_{Rf}} \sigma_{0,Rf}, \quad (2)$$

where reaction rates for bare and cadmium covered targets are represented as R and R_{Cd} , respectively. The subscripts S and Rf are used to indicate the sample under study and the reference monitor respectively. Here, g is the Westcott correction factor accounting the deviation of cross section from $1/\nu$ behaviour and $\sigma_{0,Rf}$ is the thermal cross section of reference monitor used. F_{Cd} is cadmium transmission

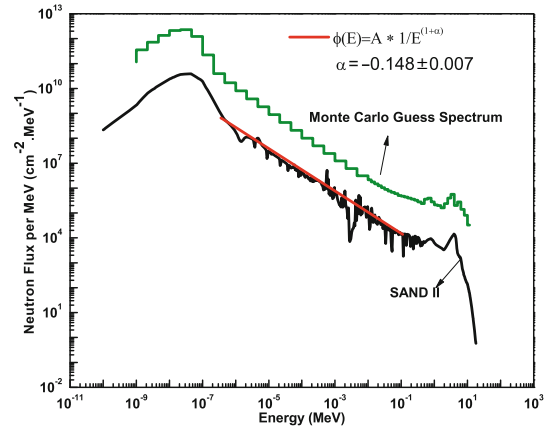


Fig. 2. Neutron spectrum unfolded using SAND II code. Epithermal spectrum fit line used to determine α is shown in bold line. The guess spectrum used for SAND II is also shown.

factor which accounts for the specific count rate difference due to cadmium cover. The spectrum-dependent resonance integral for a real spectrum (with $\frac{1}{E^{1+\alpha}}$ behaviour), $I_0(\alpha)$ is estimated from the reaction rates following the formulation explained for example by De Corte *et al.* [23] as given below:

$$I_0(\alpha)_S = I_0(\alpha)_{Rf} \frac{g_S}{g_{Rf}} \frac{(\sigma_{0,S})(F_{Cd}CR - 1)_{Rf}}{(\sigma_{0,Rf})(F_{Cd}CR - 1)_S} \times \left(\frac{G_{epi}}{G_{th}} \right)_{Rf} \left(\frac{G_{th}}{G_{epi}} \right)_S, \quad (3)$$

where CR is the ratio of reaction rates (R/R_{Cd}), and $I_0(\alpha)_{Rf}$ is the real resonance integral of reference monitor. The ideal resonance integral (I_0) of the sample is estimated from the spectrum dependent quantity $I_0(\alpha)$ using eq. (4)

$$I_0(\alpha) = (1 \text{ eV})^\alpha \frac{I_0 - 0.426\sigma_0}{(E_r)^\alpha} + \frac{0.426\sigma_0}{(2\alpha + 1)(E_{Cd})^\alpha}, \quad (4)$$

where E_r is the effective resonance energy, E_{Cd} is the cadmium cut off energy and 1 eV is the reference energy. $I_0 - 0.426\sigma_0$ is known as reduced resonance integral where the contribution from $1/\nu$ tail is eliminated. This relation is valid for $E_{Cd} = 0.55$ eV since the value 0.426 is obtained from $2(E_0/E_{Cd})^{0.5}$, where $E_0 = 0.025$ eV. Equation (4) is used to estimate the spectrum-dependent resonance integral of the reference monitors from the corresponding known ideal resonance integrals. Then eq. (3) and eq. (4) are used to obtain the $I_0(\alpha)$ and I_0 of the samples studied.

4 Measured thermal-capture cross sections and resonance integrals —results and discussions

The experimental uncertainties in the thermal-capture cross section measurements and resonance integral measurements are listed in table 3 and table 4, respectively.

Table 3. Relative uncertainties (%) of various parameters that contribute to the total uncertainty of the thermal-capture cross section estimation.

Sources of uncertainty	⁵⁵ Mn	¹⁹⁷ Au	¹³⁸ Ba	¹⁴¹ Pr
Counting Statistics (ΔC)	2.87	0.74	3.41	2.23
Half life ($\Delta T_{1/2}$)	0.01	0.04	0.34	0.21
Gamma emission probability (ΔI_γ)	0.30	0.06	1.01	10
Detector dead time	0.1	0.1	0.1	0.1
Detector efficiency ($\Delta \epsilon$)	2.4	2	1.8	3
Sample mass (Δm)	0.5	0.5	0.2	0.2
Isotopic abundance ($\Delta \theta$)	–	–	0.59	–
Monitor cross section	0.37	0.09	–	–
Section ($\Delta \sigma_{0,Rf}$)				
Self-shielding correction factor (ΔG_{th})	0.4	0.8	0.9	1.0
Total uncertainty	3.83	2.34	4.15	10.72

The relative uncertainties in the resonance integral measurements are multiplied by the error propagation factor due to the nonlinear dependency of various parameters [24]. Major sources of uncertainty in the present measurements are counting statistics and detector efficiency. Error obtained from Monte Carlo simulations are taken as the uncertainties in the self-shielding correction factors. It is seen that use of ⁵⁵Mn reference results in a higher uncertainty arising from the counting statistics due to the smaller weight of sample. There exists a large uncertainty of 10% in the gamma yield of ¹⁴²Pr (3.7 ± 0.4). Thus the overall uncertainties in the estimation of thermal-capture cross section and resonance integrals of ¹⁴¹Pr are always greater than 10%. The overall uncertainty in the case of ¹³⁹Ba is between 5%–8%. The thermal-neutron capture cross section and resonance integral values obtained from the present measurements are compared with other literature values and listed in table 5. Literature values include both experimental measurements using reactor neutron flux as well as evaluations.

4.1 ¹³⁸Ba(n, γ)¹³⁹Ba

The presently measured thermal cross section for ¹³⁸Ba with respect to ⁵⁵Mn is 0.410 ± 0.023 b and with respect to ¹⁹⁷Au is 0.386 ± 0.019 b. Similarly, the resonance integral for ¹³⁸Ba with respect to ⁵⁵Mn is 0.380 ± 0.033 b and with respect to ¹⁹⁷Au is 0.364 ± 0.027 b. The above results are average values obtained from different irradiations as well as repeated counting. The thermal-neutron capture cross section for ¹³⁸Ba determined relative to ⁵⁵Mn is in agreement with the recent experimental measurement and with the evaluated values (1.48%) and the agreement in the measurement with reference to ¹⁹⁷Au is 4.5%. The agreement with other experimental values are between 8%–40% with ⁵⁵Mn reference monitor and are between 7%–43% with ¹⁹⁷Au reference monitor except with that

reported by Lyon *et al.* [29] (78% and 68%). It is observed that the resonance integral value for ¹³⁸Ba obtained from the present study using ⁵⁵Mn reference is comparable with the recent experimental values with deviations 0.5% and using ¹⁹⁷Au reference is 4.7% [4, 30]. All other experimental values are from old experiments and hence the deviations with the present values are also varying between 18%–48%. In addition, the uncertainty in the measurement reported by Heft [31] is more than 10%. The present measurement with reference to ¹⁹⁷Au is in agreement with various reported values between 4%–38%. All the available evaluations deviates from the recent measurements. However, the Q value (I_0/σ_0) obtained in the case ⁵⁵Mn reference (0.92 ± 0.09) and in the case of ¹⁹⁷Au reference (0.94 ± 0.08) are in reasonable agreement to the recently reported value 1.04 ± 0.3 [14] within the uncertainty. It is observed that the thermal-capture cross section as well as the resonance integral estimated with respect to ⁵⁵Mn reference is greater than those estimated with respect to ¹⁹⁷Au reference. However, they are in agreement with each other within the uncertainty.

4.2 ¹⁴¹Pr(n, γ)¹⁴²Pr

The thermal-neutron capture cross section and resonance integral values obtained from the present measurements for ¹⁴¹Pr are compared with other literature values in table 5. The measured thermal cross section for ¹⁴¹Pr with respect to ⁵⁵Mn is 11.36 ± 1.29 b and with respect to ¹⁹⁷Au is 10.43 ± 1.14 b. Similarly, the resonance integral for ¹⁴¹Pr with respect to ⁵⁵Mn is 21.05 ± 2.88 b and with respect to ¹⁹⁷Au is 15.27 ± 1.87 b. The estimated thermal-neutron cross sections in the present measurement using ⁵⁵Mn and ¹⁹⁷Au reference monitors are in good agreement with each other (8.2%). The thermal-neutron capture cross sections estimated relative to ⁵⁵Mn and ¹⁹⁷Au standard are in agreement with the reported value by Yoon *et al.* [10] by 2% and 10%, respectively. They are in agreement with the evaluated and recommended data by 1.2% and 9.3%. The estimated values with reference to ⁵⁵Mn and the evaluated values are in good agreement within the experimental uncertainty. The deviations from the other experimental values are between 1%–33% (most of the values are between 1%–12%) when the reference is ⁵⁵Mn and are less than 24% when the reference is ¹⁹⁷Au. The reported resonance integrals of ¹⁴¹Pr are scattered over a range starting from 9.3 b to 21.4 b. The deviation of the present estimation with the other reported values vary from 2% to 126% in the case ⁵⁵Mn reference and from 1% to 64% in the case of ¹⁹⁷Au reference. This is due to the wide spread in the reported data. However, the resonance integral estimated in the present work reference to ¹⁹⁷Au is comparable with various evaluations within 12% to 13% agreement. The estimated value with reference to ⁵⁵Mn is in good agreement with the 1974 measurement (1.6%) [32] though the deviation from various evaluations are 19%–21%. The Q value obtained are 1.85 ± 0.33 and 1.46 ± 0.24 relative to ⁵⁵Mn and ¹⁹⁷Au, respectively, and are comparable with the recently reported value 1.41 ± 0.07 within the uncertainty [14].

Table 4. Relative uncertainties (%) of various parameters that contribute to the total uncertainty in the resonance integral estimation. Reference monitors are indicated in the parenthesis along with the sample.

Sources of uncertainty	$^{138}\text{Ba}[^{55}\text{Mn}]$	$^{138}\text{Ba}[^{197}\text{Au}]$	$^{141}\text{Pr}[^{55}\text{Mn}]$	$^{141}\text{Pr}[^{197}\text{Au}]$
α -shaping parameter ($\Delta\alpha$)	1.6	3.2	0.23	2.09
Cadmium cut-off energy (ΔE_{Cd})	0.11	0.15	0.22	0.18
Cadmium ratio of reference ($\Delta F_{Cd,Rf}$)	2.77	0.30	3.61	0.42
Cadmium ratio of sample ($\Delta F_{Cd,S}$)	2.5	2.5	3.23	3.12
Thermal-capture cross section of reference ($\Delta\sigma_{0,Rf}$)	0.09	0.04	0.02	0.03
Thermal-capture cross section of sample ($\Delta\sigma_{0,S}$)	6.50	5.8	11.38	10.97
Resonance integral of reference ($\Delta I_{0,Rf}$)	3.82	1.25	4.98	1.56
Thermal self-shielding correction factor of reference ($\Delta G_{th,Rf}$)	0.18	0.35	0.09	0.23
Thermal self-shielding correction factor of sample ($\Delta G_{th,S}$)	0.40	0.40	0.22	0.22
Epithermal self-shielding correction factor of reference ($\Delta G_{epi,Rf}$)	1.03	1.86	1.35	2.32
Epithermal self-shielding correction factor of sample ($\Delta G_{epi,S}$)	0.82	0.82	2.70	2.70
Effective resonance energy of reference ($\Delta E_{r,Rf}$)	0.71	0.68	0.92	0.85
Effective resonance energy of sample ($\Delta E_{r,S}$)	0.25	0.25	0.45	0.45
Total uncertainty	8.70	7.53	13.71	12.27

Table 5. Comparison of thermal-neutron capture cross section and resonance integral of $^{138}\text{Ba}(n,\gamma)^{139}\text{Ba}$ and $^{141}\text{Pr}(n,\gamma)^{142}\text{Pr}$ obtained from the present study with other measurements and evaluations.

Reference	$^{138}\text{Ba}(n,\gamma)^{139}\text{Ba}$		$^{141}\text{Pr}(n,\gamma)^{142}\text{Pr}$		Monitor
	σ_0 (b)	I_0 (b)	σ_0 (b)	I_0 (b)	
Present work	0.386 ± 0.019	0.364 ± 0.027	10.43 ± 1.14	15.27 ± 1.87	^{197}Au
Present work	0.410 ± 0.023	0.380 ± 0.033	11.36 ± 1.29	21.05 ± 2.88	^{55}Mn
Dauenhauer (2012) [30]	0.404 ± 0.018	0.382 ± 0.020	–	–	^{197}Au
Agbemava (2011) [4]	0.530 ± 0.010	0.380 ± 0.007	–	–	^{55}Mn
Yoon (2003) [10]	–	–	11.6 ± 1.3	–	^{197}Au
Knopf <i>et al.</i> (1997) [33]	–	–	12.7 ± 0.6	–	–
Heft (1978) [31]	0.447 ± 0.007	0.256 ± 0.050	8.36 ± 0.1	10.47 ± 0.2	^{45}Sc
Van Der Linden <i>et al.</i> (1974) [32]	–	0.330 ± 0.020	–	21.4 ± 1.8	^{197}Au
Stennes (1972) [34]	–	–	–	14.1 ± 0.12	^{197}Au
Zimmerman <i>et al.</i> (1967) [35]	–	–	11.5 ± 1	–	Transmission Method
Kramer <i>et al.</i> (1965) [36]	0.360 ± 0.036	–	–	–	^{197}Au
Lyon (1960) [29]	0.230 ± 0.023	–	10.9	–	^{55}Mn
Fehr <i>et al.</i> (1960) [37]	–	–	9.2 ± 1	15.1 ± 3	^{59}Co
Macklin (1956) [38]	–	–	–	11.3	^{197}Au
Pomerance (1952) [39]	0.680 ± 0.102	–	–	–	^{197}Au
Pomerance (1951) [40]	–	–	11.2 ± 0.6	–	^{197}Au
Harris (1950) [41]	–	–	–	9.3	^{197}Au
Seren <i>et al.</i> (1947) [42]	0.511 ± 0.102	–	10.1 ± 2.02	–	^{55}Mn , ^{115}In
Mughabghab (2006) [7]	0.404 ± 0.04	0.320 ± 0.040	11.5 ± 0.3	17.4 ± 2	Evaluations
ENDF-B.VII(1) [8]	0.404	0.265	11.5	17.85	Evaluations
EAF [9]	0.359	0.263	11.49	17.94	Evaluations

The presently measured thermal cross section of ^{138}Ba is within the range of previous measurements having a wide range as well as evaluations. However, there is no clear agreement between measurements and evaluations which indicates a need for more study. As far as present measurement of thermal cross section of ^{141}Pr is concerned, there is a good agreement between other measurements and the evaluated data. Resonance integral measured for ^{138}Ba with respect to ^{55}Mn shows good agreement with recent measurements, but different from evaluations thus showing the need for revising the evaluations. The present measurements for resonance integral of ^{141}Pr is found to be supported by the evaluations rather than the other measurements which are relatively old.

5 Summary

The thermal cross sections and the resonance integrals for $^{138}\text{Ba}(n, \gamma)^{139}\text{Ba}$ and $^{141}\text{Pr}(n, \gamma)^{142}\text{Pr}$ are measured using an isotopic Am-Be source. The measured thermal cross section for ^{138}Ba with respect to ^{55}Mn is 0.410 ± 0.023 b and with respect to ^{197}Au is 0.386 ± 0.019 b. The resonance integral for ^{138}Ba with respect to ^{55}Mn is 0.380 ± 0.033 b and with respect to ^{197}Au is 0.364 ± 0.027 b. The measured thermal cross section for ^{141}Pr with respect to ^{55}Mn is 11.36 ± 1.29 b and with respect to ^{197}Au is 10.43 ± 1.14 b. The resonance integral for ^{141}Pr with respect to ^{55}Mn is 21.05 ± 2.88 b and with respect to ^{197}Au is 15.27 ± 1.87 b.

Although, the thermal cross section of ^{138}Ba from the present study compares with one of the recently reported values [30], the difference among various evaluations and measurements indicate the need for further study. In the case of resonance integral measurements of ^{138}Ba , the discrepancy between the evaluations [7–9] and new measurements [4, 30] including the present study can be attributed to the pre dated evaluations compared to the measurements. This observation suggests the need for revising the evaluations. Various evaluations and measurements support the thermal cross section of ^{141}Pr measured in the present study. Present measurement of resonance integral of ^{141}Pr is in agreement with various evaluations. There has been no other recent measurement of resonance integral and older measurements show an unacceptably high spread. However, uncertainties in the thermal cross sections and resonance integrals of ^{141}Pr are more than 10% due to the larger uncertainty in the γ branching ratio of ^{142}Pr . The following conclusions are drawn from the present study.

- The present study proves the viability of a high intense Am-Be isotopic source placed in a thick concrete bunker for thermal cross section and resonance integral measurements.
- The Monte Carlo based self-shielding correction are more suited to account for changes in irradiation channel.
- The presently reported thermal-neutron capture cross section for ^{138}Ba and ^{141}Pr are in reasonable agreement with the evaluated data available. However, the

old evaluated resonance integral data need to be revised taking into account recently available data including the present measurements.

The authors are thankful to Dr. V. Gopalakrishnan and Dr. M. Gupta, Manipal Centre for Natural Sciences for their valuable suggestions during various stages of the present work.

References

1. M. Barbagallo *et al.*, EPJ Web of Conferences **66**, 10001 (2014).
2. S. Ganesan, Nucl. Data Sheets **123**, 21 (2015).
3. M. Calviani *et al.*, in *International Conference on Nuclear Data for Science and Technology*, Vol. **335** (EDP Sciences, 2007).
4. S.E. Agbemava, R.B.M. Sogbadji, B.J.B. Nyarko, R. Della, Ann. Nucl. Energy **38**, 379 (2011).
5. M. Karadag, Ann. Nucl. Energy **62**, 274 (2013).
6. N. Otuka *et al.*, Nucl. Data Sheets **120**, 272 (2014).
7. S.F. Mughabghab, *Atlas of Neutron Resonances: Resonance Parameters and Thermal Cross Sections. Z = 1–100* (Elsevier, 2006).
8. M.B. Chadwick *et al.*, Nucl. Data Sheets **112**, 2887 (2011).
9. J.-Ch. Sublet, L.W. Packer, J. Kopecky, R.A. Forrest, A.J. Koning, D.A. Rochman, *The european activation file: EAF-2010 neutron-induced cross section library*, CCFE Report R **10**, 5 (2010).
10. J. Yoon, S. Lee, S. Yamamoto, K. Kobayashi, T. Ro, J. Nucl. Sci. Technol. **40**, 447 (2003).
11. M.J. Berger, J.H. Hubbell, S.M. Seltzer, J. Chang, J.S. Coursey, R. Sukumar, D.S. Zucker, K. Olsen, *Xcom: Photon cross sections database*, NIST Standard reference database 8 (2013).
12. F. De Corte, A. Simonits, At. Data Nucl. Data Tables **85**, 47 (2003).
13. R.B. Firestone, V.S. Shirley, C.M. Baglin, S.Y. Frank Chu, J. Zipkin, *Table of Isotopes*, 8th edition (John Wiley & Sons, New York, 1996).
14. F. Farina, P. Vermaercke, K. Smits, L. Sneyers, K. Strijckmans, J. Radioanal. Nucl. Chem. **296**, 931 (2013).
15. B. Pritychenko, S.F. Mughabghab, Nucl. Data Sheets **113**, 3120 (2012).
16. *Neutron Fluence Measurements*, IAEA Technical Reports Series No. **107** (IAEA, Vienna, 1970).
17. M. Blaauw, Nucl. Instrum. Methods Phys. Res. A **356**, 403 (1995).
18. E. Martinho, I.F. Gonçalves, J. Salgado, Appl. Radiat. Isotopes **58**, 371 (2003).
19. N. Van Do *et al.*, Nucl. Instrum. Methods Phys. Res. B **267**, 462 (2009).
20. J.F. Briesmeister *et al.*, *MCNP—A general Monte Carlo code for neutron and photon transport* (Los Alamos National Laboratory, 1986).
21. A. Trkov, G. Žerovnik, L. Snoj, M. Ravnik, Nucl. Instrum. Methods Phys. Res. A **610**, 553 (2009).
22. A. Koning *et al.*, *The JEFF-3.1 nuclear data library* (OECD, 2006).
23. F. De Corte, K.Sordo-El Hammami, L. Moens, A. Simonits, A. De Wispelaere, J. Hoste, J. Radioanal. Chem. **62**, 209 (1981).

24. H. Yücel, M. Karadag, Ann. Nucl. Energy **31**, 681 (2004).
25. M.U. Rajput, M. Ahmad, W. Ahmad, Phys. Rev. C **68**, 044608 (2003).
26. F. De Corte, L. Moens, S. Jovanović, A. Simonits, A. De Wispelaere, J. Radioanal. Nucl. Chem. **102**, 37 (1986).
27. W.N. McElroy, *A computer-automated iterative method for neutron flux spectra determination by foil activation* (1967).
28. D.K. Mohapatra, E. Radha, P. Mohanakrishnan, Ann. Nucl. Energy **31**, 197 (2004).
29. W.S. Lyon, Nucl. Sci. Engin. **8**, 378 (1960).
30. A.Y. Dauenhauer, K.S. Krane, Phys. Rev. C **85**, 064301 (2012).
31. R.E. Heft, *A consistent set of nuclear-parameter values for absolute INAA*, in *Conference on Computers in Activation Analysis and Gamma-ray Spectroscopy, Mayaguez, Puerto Rico, 30 Apr - 4 May 1978*, edited by B.S. Carpenter *et al.* (Department of Energy, Washington, DC, 1979) pp. 495–510; UCRL-80286, Lawrence Livermore Laboratory, California (1978).
32. R. Van der Linden, F. De Corte, J. Hoste, J. Radioanal. Chem. **20**, 695 (1974).
33. K. Knopf, W. Waschkowski, Z. Phys. A **357**, 297 (1997).
34. E. Steignes, J. Inorg. Nucl. Chem. **34**, 2699 (1972).
35. R.L. Zimmerman, L.Q. Amaral, R. Fulfaro, M.C. Mattos, M. Abreu, R. Stasiulevicius, Nucl. Phys. A **95**, 683 (1967).
36. H.H. Kramer, W.H. Wahl, Nucl. Sci. Engin. **22**, 373 (1965).
37. E. Fehr, E. Hansen, Knolls Atomic Power Lab., Rep. Ser. **2000**, 12 (1960).
38. R.L. Macklin, H.S. Pomerance, *Resonance Capture Integrals*, in *Proceedings of the 1st United Nations International Conference on Peaceful Uses of Atomic Energy, Geneva, 1955*, Vol. **5** (United Nations, New York, 1956) p. 96.
39. H. Pomerance, Phys. Rev. **88**, 412 (1952).
40. H. Pomerance, Phys. Rev. **83**, 641 (1951).
41. S.P. Harris, C.O. Muehlhause, G.E. Thomas, Phys. Rev. **79**, 11 (1950).
42. L. Seren, H.N. Friedlander, S.H. Turkel, Phys. Rev. **72**, 888 (1947).